Planar Dynamics of a Motorcycle with Electric Powertrain: Modeling Inertia Effect of Mounting System

Sudhir Kaul

Department of Mechanical Engineering, Milwaukee School of Engineering, Milwaukee, WI, 53202, USA. Email: kaul@msoe.edu

(Received 5 February 2025; accepted 1 June 2025)

This paper examines the planar (in-plane) dynamics of a motorcycle with a specific focus on modeling the influence of the inertia effect of the mounting system of an electric powertrain. The inertia effect of the mounting system is examined by capturing wave effects and internal resonances of the vibration isolation system through a discretized model that is capable of high frequency characterization. Since an electric drive system exhibits vibroacoustic characteristics that are significantly different from an internal combustion engine, the model is particularly aimed at analyzing the planar dynamics of a motorcycle with an electric powertrain. The specific contribution of this paper is the integration of a discretized model of the mounting system with the planar model of the motorcycle. The planar model has been used to evaluate ride comfort and handling when the motorcycle is traveling in a straight line. Results indicate that the model can capture internal resonances of the mounting system at relatively higher frequencies (above 1 kHz) that may not be possible with a conventional spring-damper representation. The planar model presented in this paper is comprehensive and can be adapted to investigate critical design parameters associated with the mounting and suspension systems in motorcycles with electric powertrains.

NOMENCLATURE

θ	Sprung mass pitch
γ	Powertrain pitch
p	Motorcycle wheelbase
b	Distance from center of mass of sprung mass to point of contact of rear tire
$x_{r1}, y_{r1}, x_{f1}, y_{f1}$	Location of elastic center of front engine mount and rear engine mount from center of mass of powertrain
y, y_f, y_r, y_p	Vertical displacements of the sprung mass, front unsprung mass, rear unsprung mass, and powertrain respectively
$z_{1fy}, \ldots, z_{Nfy}$; $z_{1ry}, \ldots, z_{Nry}$; $z_{1fx}, \ldots, z_{Nfx}$; $z_{1rx}, \ldots, z_{Nrx}$	Displacements of discretized elements of the mounting system
c_f, c_r	Equivalent damping constants of front and rear suspension respectively
c_{pf}, c_{pr}	Equivalent damping constants of front and rear tire respectively
k_f, k_r	Equivalent stiffness constants of front and rear suspension respectively
k_{pf}, k_{pr}	Equivalent stiffness constants of front and rear tire respectively
m, I	Mass and mass moment of inertia of sprung mass about its center of mass
m_p, I_p	Mass and mass moment of inertia of powertrain about its center of mass
m_f, m_r	Front and rear unsprung mass respectively
$E_0, E_{\alpha x}, E_{\beta x}$, $E_{\alpha y}, E_{\beta y}$	Modulus of elasticity and non-equilibrium moduli for engine mounting system

1. INTRODUCTION

The increasing use of electric powertrains has introduced some new aspects to noise, vibration, and harshness (NVH) in motorcycle dynamics that need to be thoroughly analyzed. Motorcycle dynamics has been an active area of research for several decades,[1,2] with studies investigating aspects such as handling, maneuverability, cornering, ride comfort, etc. However, the use of electric powertrains poses alternate design requirements and constraints on the mounting systems that may not have been prevalent for internal combustion engines. The use of engine mounts (or vibration isolation systems) is not common in motorcycle powertrains except for a few commercial manufacturers who use isolators for mitigating shaking forces produced by the engine, or for isolating the frame from torque recoil, or for isolating at idling or low speeds.[3,4] Many of these factors are not critical or may not even be relevant in electric powertrains. For example, torque fluctuation is significantly lower in an electric powertrain, as a result torque recoil is not an important parameter for the mounting system. On

the other hand, the internal resonances of the mounting system may play a significant role in an electric powertrain, therefore modeling the mounts as lumped spring-damper systems may not be sufficient since such a model would not capture the inertia effects and internal resonances.[5,6] Due to these critical distinctions, it is necessary to develop updated models of mounting systems that can be integrated with the overall planar models of motorcycles with electric powertrains.

The most commonly used motors in the current designs of electric vehicles include the permanent-magnet synchronous motor (PMSM), the induction motor (IM), and the switched reluctance motor.[7] It is commonly acknowledged in the literature that electric motors exhibit high frequency harmonics that are typically related to phenomena such as electric whistling or high frequency buzz.[8–10] High frequency noise and vibration have been investigated in a PMSM through experimental evaluation and multiphysics modeling, it is observed that the harmonics of electromagnetic forces are critical contributors in the vibroacoustic response of such motors.[8] In a PMSM, electromagnetic vibroacoustics are typically associated with the interaction between the stator and the permanent magnets. The three-phase PMSM has been commonly adopted in many electric vehicles due to relatively higher efficiency and a significantly higher power-to-torque density. On the other hand, induction motors are preferred by some manufactures due to high torque density but these motors continue to remain dependent on the availability of rare earth metals that could entail relatively higher manufacturing costs.[11] Multiple other considerations are typically taken into account before selecting the appropriate electric motor for an application and can be found in detail from recent literature.[11] The rapid development of electric motorcycles by multiple manufacturers necessitates an in-depth analysis of planar dynamics due to some key distinctions between internal combustion engines and different kinds of electric powertrains.[12] This study aims to provide one such analysis.

The study of motorcycle dynamics has been significantly enabled over the last couple of decades with the availability of commercial programs such as BikeSim,[13] Fastbike,[14] etc. Most of the multibody models can be generally classified as spatial or planar. While the spatial models are typically used to investigate maneuverability, stability, cornering, and control, planar models are generally used to comprehend ride comfort and suspension characteristics at constant speeds under straight-running conditions. The planar modes are typically decoupled from the spatial modes, however specific design attributes of the planar modes can directly influence some characteristics of the spatial modes. Although the use of commercial programs is very beneficial in the overall analysis of multibody dynamics, such programs are of limited use for analyzing the integration of component-level models with the overall planar model to determine the specific attributes of components such as the design parameters of the mounting system. There are a few studies in the existing literature that have investigated the mounting layouts of electric powertrains,[15–17] while other studies have considered possible means of vibration suppression in electric powertrains.[18–20] There are additional studies in the recent literature that have focused on aspects such as rubber-metal simulations of engine mounts,[21] use of smart mounting systems made of magnetorheological materials,[22] and effects of exposure to vibration on motorcyclists.[23]

This study aims to comprehend the role of the mounting system of an electric powertrain in the planar dynamics of a motorcycle. Such a model is not available in the current literature on electric motorcycles even though there is an increasing number of electric motorcycle manufacturers.[24,25] The model developed in this study accounts for the internal resonances of the mounting system while evaluating ride comfort and in-plane handling of a motorcycle. The proposed model can be particularly useful for the analysis of key design parameters of the mounting system and the investigation of sensitivity of ride comfort and planar handling to specific variables associated with the mounting system.

In this paper, Section 2 presents the planar model along with a discussion on the main assumptions that have been used to develop this model. The proposed model has been used for analysis and results are presented in Section 3 along with a discussion of the results. Overall conclusions from the simulation results are summarized in Section 4 and possible areas of future work have also been discussed in this section.

2. MODEL — PLANAR DYNAMICS WITH INERTIA EFFECT

The governing equations of motion (EOM) for the planar model are derived in this section and the main assumptions associated with the EOM are discussed along with an overall description of the model. The planar model was divided into four rigid bodies — sprung mass (chassis and rider together), front unsprung mass, rear unsprung mass, and powertrain. This distribution of rigid bodies was like other studies in the literature that investigate the planar dynamics of motorcycles.[2,4] The four rigid bodies were interconnected either through the suspension system or the mounting system. Each suspension system was represented as a spring-damper unit while each engine mount was modeled as a discretized chain of lumped masses that were interconnected through a series of viscoelastic elements. Such a representation of the engine mounts enables the model to capture internal resonance effects that are essential for capturing high frequency response and wave effects typically associated with electric powertrains.[5,25] Two horizontal mounts and two vertical mounts were used in the model discussed in this study, and the layout of the entire model can be seen in Figure 1. It may be noted that the model was not limited to two engine mounts, a varying number of mounts and mounting layouts can be accommodated in the model presented in this study.

The powertrain was modeled with three planar degrees-of-freedom. The governing EOM of the powertrain are derived as follows:

$$m_p\ddot{x}_p = -F_{sa}\cos\varphi - F_{fx} - F_{rx}; \tag{1}$$

$$m_p\ddot{y}_p = -F_{sa}\sin\varphi - F_{fy} - F_{ry}; \tag{2}$$

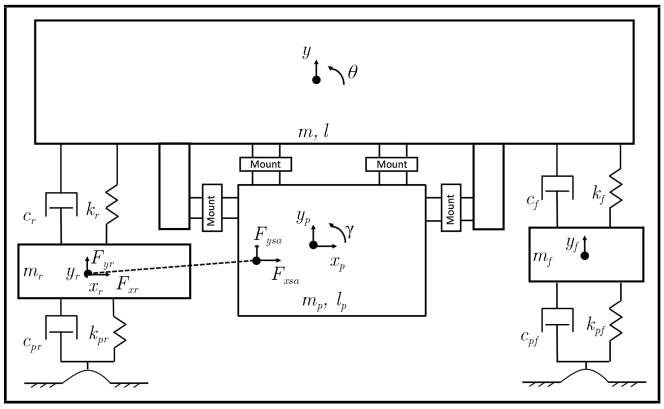

Figure 1. Eight degree-of-freedom planar model.

$$I_p\ddot{\gamma} = F_{fx}y_{f1} - F_{fy}x_{f1} - F_{rx}y_{r1} + F_{ry}x_{r1} - F_{sa}\cos\varphi y_{sa} + F_{sa}\sin\varphi x_{sa}. \quad (3)$$

In Eqs. (1)–(3), F_{fx}, F_{fy}, F_{rx}, and F_{ry} were the time varying dynamic forces at the front and rear mounting points of the powertrain in the horizontal and vertical directions while x_p, y_p, and γ were the three degrees-of-freedom of the powertrain. The position of the mounts was identified at the elastic center of each mount with respect to the center of mass of the powertrain. The front and rear mounts were located at (x_{f1}, y_{f1}) and (x_{r1}, y_{r1}) respectively while (x_{sa}, y_{sa}) was the location of the swing arm connection point from the center of mass of the powertrain. Also, m_p was the mass of the powertrain while I_p was the mass moment of inertia of the powertrain along the z-axis about its center of mass. Furthermore, F_{sa} was the reaction force at the powertrain due to the swing arm connection between the powertrain and the rear axle and φ was the angle of inclination of the swing arm from the horizontal axis. It may be noted that this angle of inclination varies with the overall trim and may change to a limited extent with the rear wheel hop.

To capture the internal resonances of the mounting system, each mount was modeled as a chain of (N) lumped masses in series connected through viscoelastic elements. For an engine mount with an overall mass of m_e, each lumped mass was discretized such that $\overline{m} = \frac{m_e}{N}$. For simplicity, the front and rear mounts were assumed to be identical so that the viscoelastic elements of the mounts were identical, $k_{1fy} = k_{1ry} = k_y$ and $k_{1fx} = k_{1rx} = k_x$. A representation of one of the discretized engine mounts between the powertrain and the sprung mass is shown in Figure 2. The number of discretized elements can be determined by using a convergence criterion or an experimental evaluation.

The dynamic forces at the front and rear mounting points on the powertrain can be expressed as:

$$F_{fy} = k_{1fy}\left(y_p + x_{f1}\gamma - z_{1fy}\right); \quad (4)$$

$$F_{fx} = k_{1fx}\left(x_p - y_{f1}\gamma - z_{1fx}\right); \quad (5)$$

$$F_{ry} = k_{1ry}\left(y_p - x_{r1}\gamma - z_{1ry}\right); \quad (6)$$

$$F_{rx} = k_{1rx}\left(x_p + y_{r1}\gamma - z_{1rx}\right). \quad (7)$$

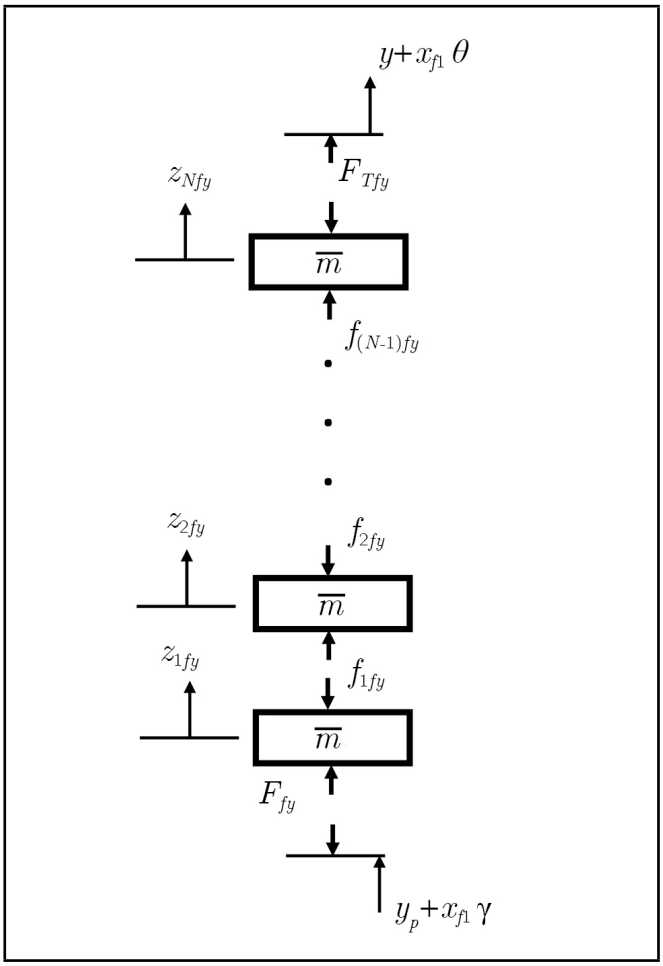

Figure 2. Discretized engine mount model — front mount — vertical.

In Eqs. (4)–(7), k_{1fy}, k_{1fx}, k_{1ry}, k_{1rx} represented the effective stiffness of the viscoelastic elements connecting the lumped masses together, as shown in the discretized engine mount model in Figure 2. For identical cylindrical engine mounts in compression, $k_{1fy} = k_{1ry} = k_y = \frac{(N_y+1)A_yE_y}{h_y}$ and $k_{1fx} = k_{1rx} = k_x = \frac{(N_x+1)A_xE_x}{h_x}$, where A_y and A_x are the cross-sections of the cylindrical engine mounts, and h_y and h_x were the heights of the cylindrical mounts while E_y and E_x were the complex moduli of the elastomeric material. For the two-fractional element model, $E_y = E_0 + E_{\alpha y}(i\omega\tau)^{\alpha} + E_{\beta y}(i\omega\tau)^{\beta}$ and $E_x = E_0 + E_{\alpha x}(i\omega\tau)^{\alpha} + E_{\beta x}(i\omega\tau)^{\beta}$. For the complex moduli, E_0 was the modulus of elasticity of the elastomeric material, τ was the time constant, α and β were fractional orders, and $E_{\alpha y}$, $E_{\alpha x}$, $E_{\beta y}$, $E_{\beta x}$ were the non-equilibrium moduli. Also, N_y and N_x were the number of elements used to represent the vertical and horizontal engine mounts, the number of elements of the discretized model can be determined iteratively by using a convergence criterion.[26]

Applying Fourier transform to Eqs. (1)–(3) and substituting the dynamic forces from Eqs.(4)–(7) results in the following equations in the frequency domain:

$$-\omega^2 m_p X_p + 2k_x X_p + \left(-k_x y_{f1} + k_x y_{r1}\right)\Gamma = -F_{sa}\cos\varphi + k_x Z_{1fx} + k_x Z_{1rx}; \quad (8)$$

$$-\omega^2 m_p Y_p + 2k_y Y_p + (k_y x_{f1} - k_y x_{r1})\,\Gamma = -F_{sa}\sin\varphi + k_y Z_{1fy} + k_y Z_{1ry}; \quad (9)$$

$$-\omega^2 I_p \Gamma + \left(k_x y_{f1}^2 + k_y x_{f1}^2 + k_x y_{r1}^2 + k_y x_{r1}^2\right)\Gamma + (-k_x y_{f1} + k_x y_{r1})\,X_p + (k_y x_{f1} - k_y x_{r1})\,Y_p = -F_{sa}\cos\varphi y_{sa} + F_{sa}\sin\varphi x_{sa} - k_x y_{f1} Z_{1fx} + k_y x_{f1} Z_{1fy} + k_x y_{r1} Z_{1rx} - k_y x_{r1} Z_{1ry}. \quad (10)$$

The EOM of the discretized engine mounts at the front and rear ends of the powertrain can be derived for the first element ($j = 1$), the intermediate elements ($j = 2, \cdots, N-1$), and the last element ($j = N$). For the first discretized element ($j = 1$) that was connected at the powertrain end, the EOM were derived as:

$$\overline{m}\ddot{z}_{1ry} = F_{ry} - f_{1ry}; \quad (11)$$

$$\overline{m}\ddot{z}_{1fy} = F_{fy} - f_{1fy}; \quad (12)$$

$$\overline{m}\ddot{z}_{1rx} = F_{rx} - f_{1rx}; \quad (13)$$

$$\overline{m}\ddot{z}_{1fx} = F_{fx} - f_{1fx}. \quad (14)$$

The EOM for the discretized elements can be generalized for the series of intermediate elements, $j = 2, \cdots, N-1$, as follows:

$$\overline{m}\ddot{z}_{jry} = f_{(j-1)ry} - f_{jry}; \quad (15)$$

$$\overline{m}\ddot{z}_{jfy} = f_{(j-1)fy} - f_{jfy}; \quad (16)$$

$$\overline{m}\ddot{z}_{jrx} = f_{(j-1)rx} - f_{jrx}; \quad (17)$$

$$\overline{m}\ddot{z}_{jfx} = f_{(j-1)fx} - f_{jfx}. \quad (18)$$

In Eqs. (15)–(18), $f_{jfy} = k_y\left(z_{jfy} - z_{(j+1)fy}\right)$, $f_{jry} = k_y\left(z_{jry} - z_{(j+1)ry}\right)$, $f_{jfx} = k_x\left(z_{jfx} - z_{(j+1)fx}\right)$, and $f_{jrx} = k_x\left(z_{jrx} - z_{(j+1)rx}\right)$ for $j = 1, \cdots, N-1$.

Finally, the EOM for the last discretized element ($j = N$) connecting the mount to the sprung mass were:

$$\overline{m}\ddot{z}_{Nry} = f_{(N-1)ry} - F_{Try}; \quad (19)$$

$$\overline{m}\ddot{z}_{Nfy} = f_{(N-1)fy} - F_{Tfy}; \quad (20)$$

$$\overline{m}\ddot{z}_{Nrx} = f_{(N-1)rx} - F_{Trx}; \quad (21)$$

$$\overline{m}\ddot{z}_{Nfx} = f_{(N-1)fx} - F_{Tfx}. \quad (22)$$

In Eqs. (19)–(22), $F_{Tfy} = k_y\left(z_{Nfy} - y - x_{f1}\theta\right)$, $F_{Try} = k_y\left(z_{Nry} - y + x_{r1}\theta\right)$, $F_{Tfx} = k_x z_{Nfx}$, and $F_{Trx} = k_x z_{Nrx}$, represented the forces transmitted to the sprung mass through the last discretized element. Furthermore, in Eqs. (7)–(22), z_{jfy}, z_{jry}, z_{jfx}, and z_{jrx} represent translation of the discretized elements used to represent the front and rear engine mounts in the vertical and horizontal directions as $j = 1, \cdots, N$.

Applying the Fourier transform to Eqs. (11)–(22) yields the frequency response of the discretized elements of the mounting system as follows:

$$\left(2k_y - \overline{m}\omega^2\right) Z_{1ry} - k_y Z_{2ry} = k_y Y_p - k_y x_{r1}\Gamma; \quad (23)$$

$$\left(2k_y - \overline{m}\omega^2\right) Z_{1fy} - k_y Z_{2fy} = k_y Y_p + k_y x_{f1}\Gamma; \quad (24)$$

$$\left(2k_x - \overline{m}\omega^2\right) Z_{1rx} - k_x Z_{2rx} = k_x X_p + k_x y_{r1}\Gamma; \quad (25)$$

$$\left(2k_x - \overline{m}\omega^2\right) Z_{1fx} - k_x Z_{2fx} = k_x X_p - k_x y_{f1}\Gamma; \quad (26)$$

$$\left(2k_y - \overline{m}\omega^2\right) Z_{jry} - k_y Z_{(j-1)ry} - k_y Z_{(j+1)ry} = 0; \quad (27)$$

$$\left(2k_y - \overline{m}\omega^2\right) Z_{jfy} - k_y Z_{(j-1)fy} - k_y Z_{(j+1)fy} = 0; \quad (28)$$

$$\left(2k_x - \overline{m}\omega^2\right) Z_{jrx} - k_x Z_{(j-1)rx} - k_x Z_{(j+1)rx} = 0; \quad (29)$$

$$\left(2k_x - \overline{m}\omega^2\right) Z_{jfx} - k_x Z_{(j-1)fx} - k_x Z_{(j+1)fx} = 0; \quad (30)$$

$$\left(2k_y - \overline{m}\omega^2\right) Z_{Nry} - k_y Z_{(N-1)ry} = k_y Y - k_y x_{r1}\Theta; \quad (31)$$

$$\left(2k_y - \overline{m}\omega^2\right) Z_{Nfy} - k_y Z_{(N-1)fy} = k_y Y + k_y x_{f1}\Theta; \quad (32)$$

$$\left(2k_x - \overline{m}\omega^2\right) Z_{Nrx} - k_x Z_{(N-1)rx} = 0; \quad (33)$$

$$\left(2k_x - \overline{m}\omega^2\right) Z_{Nfx} - k_x Z_{(N-1)fx} = 0. \quad (34)$$

Overall, Eqs. (23)–(34) represent the frequency response of all the discretized elements, and $j = 2, \cdots, N-1$ in Eqs. (27)–(30). It may be noted that $Y(\omega)$ and $\Theta(\omega)$ represented the frequency response of the two degrees-of-freedom of the sprung mass in time domain — $y(t)$ and $\theta(t)$ respectively. The frequency response was coupled to the rest of the system since the engine mounts were assembled between the sprung mass and the powertrain. The frequency response of the sprung mass, rear unsprung mass, and front unsprung mass was derived from the governing EOM of the three rigid bodies. The frequency response of the sprung mass was derived as:

$$-m\omega^2 Y + j\omega\,(c_f + c_r)\,Y + (k_f + k_r + 2k_y)\,Y + j\omega\,[c_f(p-b) - c_r b]\,\Theta + [k_f(p-b) - k_r b + k_y x_{f1} - k_y x_{r1}]\,\Theta - j\omega c_f Y_f - j\omega c_r Y_r - k_f Y_f - k_r Y_r = k_y\,(Z_{Nfy} + Z_{Nry}); \quad (35)$$

$$-I\omega^2\Theta + j\omega\left[c_f(p-b)^2 + c_r b^2\right]\Theta + \left[k_f(p-b)^2 + k_r b^2 + k_y x_{f1}^2 + k_y x_{r1}^2\right]\Theta + j\omega\,[c_f(p-b) - c_r b]\,Y + [-k_r b + k_f(p-b) + k_y x_{f1} - k_y x_{r1}]\,Y - j\omega c_f(p-b)Y_f - k_f(p-b)Y_f + j\omega c_r b Y_r + k_r b Y_r = k_y\,(Z_{Nfy}x_{f1} - Z_{Nry}x_{r1}) + k_x\,(Z_{Nrx}y_1 - Z_{Nfx}y_1)\,. \quad (36)$$

In Eqs. (35) and (36), the frequency response of the vertical displacement (bounce) of the sprung mass was represented by $Y(\omega)$ and the frequency response of the in-plane (pitch) rotation of the sprung mass was represented by $\Theta(\omega)$. Also, p was the wheelbase (distance between the contact point of the front tire and the contact point of the rear tire, assuming a point contact) and b was the distance from the center of mass of the sprung mass to the contact point of the rear tire. Furthermore, (x_{r1}, y_1) identified the position of the elastic center of the rear mount while (x_{f1}, y_1) identified the elastic center of the front mount from the center of mass of the sprung mass. In Eqs. (35) and (36), k_f and c_f were the equivalent stiffness and damping constants of the front suspension while k_r and c_r

were the equivalent stiffness and damping constants of the rear suspension.[2] Also, Y_f and Y_r represented the frequency response of the hop (vertical displacement) of the front and rear unsprung mass respectively. Each unsprung mass was the combined mass of the wheel and other parts of the wheel assembly such as the tire, brake, axle, etc.

Although the powertrain mounting system was not directly connected to the unsprung masses, the dynamics of the system were coupled with the unsprung masses through the sprung mass, as seen from Eqs. (35) and (36). The frequency response of the two unsprung masses was derived as follows:

$$-\omega^2 m_r X_r = F_{sa}\cos\varphi; \tag{37}$$

$$-\omega^2 m_r Y_r + j\omega\left(c_{pr}+c_r\right)Y_r - j\omega c_r Y + j\omega c_r b\Theta + \left(k_{pr}+k_r\right)Y_r - k_r Y + k_r b\Theta = F_{sa}\sin\varphi + Y_{fi}\, e^{-j\omega\frac{p}{V}}; \tag{38}$$

$$-\omega^2 m_f Y_f + j\omega\left(c_{pf}+c_f\right)Y_f - j\omega c_f Y - j\omega c_f(p-b)\Theta + \left(k_{pf}+k_f\right)Y_f - k_f Y - k_f(p-b)\Theta = Y_{fi}. \tag{39}$$

In Eqs. (37)–(39), $X_r(\omega)$ and $Y_r(\omega)$ was the frequency response of the rear unsprung mass (m_r) while $Y_f(\omega)$ was the frequency response of the front unsprung mass (m_f). Furthermore, the equivalent stiffness and damping constants of the rear tire were k_{pr} and c_{pr} respectively while the equivalent stiffness and damping constants of the front tire were k_{pf} and c_{pf} respectively. Finally, Y_{fi} was the amplitude of excitation at the front tire due to the irregularity of the road surface while the motorcycle was traveling in a straight line at a constant speed, V.

The frequency response of the discretized mounting system was directly coupled to the degrees-of-freedom of the system. Therefore, for an input due to the irregularities of the road surface, all eight DOF were expressed in terms of the degrees-of-freedom of the discretized mounting system. This allows the determination of the frequency response of the discretized mounting system first, followed by computing the frequency response of the eight DOF of the system. For a displacement input of $y_{fi}(t)$ at the front wheel due to the irregularity of the road surface, the displacement input at the rear wheel input was $y_{fi}\left(t-\frac{p}{V}\right)$ due to the time delay between the input at the two wheels, commonly referred to as wheelbase filtering,[1,2] as the motorcycle, with a wheelbase of p, travels in a straight line with a constant speed of V. The combined frequency response of the system can be expressed as follows:

$$\begin{bmatrix} F_1 & F_2 & F_3 & F_4 & F_5 & F_6 & F_7 & F_8 \end{bmatrix} \begin{bmatrix} Y \\ \Theta \\ Y_f \\ X_r \\ Y_r \\ X_p \\ Y_p \\ \Gamma \end{bmatrix} = Z_\omega. \tag{40}$$

In Eq. (40), the right-hand side of the equation is expressed as: $Z_\omega =$

$$\begin{bmatrix} k_y\left(Z_{Nfy}+Z_{Nry}\right) \\ k_y\left(Z_{Nfy}x_{f1}-Z_{Nry}x_{r1}\right)+k_x\left(Z_{Nrx}y_1-Z_{Nfx}y_1\right) \\ k_x\left(Z_{1fx}+Z_{1rx}\right) \\ k_y\left(Z_{1fy}+Z_{1ry}\right) \\ -k_x y_{f1}Z_{1fx}+k_y x_{f1}Z_{1fy}+k_x y_{r1}Z_{1rx}-k_y x_{r1}Z_{1ry} \\ 0 \\ k_{pr}Y_{fi}e^{-j\omega\frac{p}{V}} \\ k_{pf}Y_{fi} \end{bmatrix}.$$

Furthermore, in Eq. (40), $F_1,\ F_2,\ \ldots,\ F_8$ were the columns of the matrix using $f_{sa1}, f_{sa2}, f_{sa3}$ as different components of the force transmitted through the swing arm, modeled as a pin connected structure between the unsprung mass at one end and the powertrain at the other end. The columns of the matrix on the left-hand side of Eq. (40) are listed on the top of the next page.

To use the model discussed in this section, Eq. (40) was solved in conjunction with the system of equations in Eq. (23)–(34) to determine the frequency response of the eight degrees-of-freedom along with the frequency response of the N number of discretized engine mounts. The number of discretized elements used to represent each engine mount were determined iteratively by using a convergence criterion of 5% for force transmitted to the sprung mass. For this study, the convergence criterion yielded $N = 80$, therefore the system had been solved for $4N + 8$ (total of 328 in this study) degrees-of-freedom. The force transmitted to the spung mass through the mounting system is determined as follows:

$$F_{Tx} = k_x z_{Nfx} + k_x z_{Nrx}; \tag{41}$$

$$F_{Ty} = k_y\left(z_{Nfy}-y-x_{f1}\theta\right)+k_y\left(z_{Nry}-y+x_{r1}\theta\right). \tag{42}$$

Using Eqs. (41) and (42), the norm of the force transmitted, F_T, to the sprung mass through the mounting system has been used for convergence.

To evaluate ride comfort and handling, power spectral density (PSD) of the sprung mass and unsprung masses has been calculated as:

$$S_i(\omega,\ V) = \left|H_i^*(\omega,V)\right|^2 S_r(\omega,V). \tag{43}$$

In Eq. (43), $S_r(\omega,V)$ is the PSD of the road surface over which the motorcycle is traveling in a straight line at a constant velocity, V, and $S_i(\omega,V)$ was the PSD of the i^{th} DOF while $H_i^*(\omega,V)$ was the frequency response of the system that accounts for wheelbase filtering.[4] The PSD of the road surface was a function of motorcycle velocity, nature of road surface, and frequency, and can be referenced from existing literature.[27]

The model presented in this section has a total of eight degrees-of-freedom associated with the rigid bodies shown in Figure 1. Furthermore, additional degrees-of-freedom were associated with the discretized engine mounting system. This model was used for multiple simulations in Section 3. Simulation results are discussed in Section 3 and some of the key parameters associated with the mounting system are also investigated.

$$F_1 = \left[-m\omega^2 + j\omega\left(c_f + c_r\right) + \left(k_f + k_r + 2k_y\right) \quad j\omega\left\{c_f(p-b) - c_r b\right\} + \left\{k_f(p-b) - k_r b + k_y x_{f1} - k_y x_{r1}\right\} \right.$$
$$\left. 0 \quad 0 \quad 0 \quad 0 \quad -j\omega c_r - k_r \quad -j\omega c_f - k_f\right]^T,$$
$$F_2 = \left[j\omega\left\{c_f(p-b) - c_r b\right\} + \left\{k_f(p-b) - k_r b + k_y x_{f1} - k_y x_{r1}\right\} \quad -I\omega^2 + j\omega\left\{c_f(p-b)^2 + c_r b^2\right\} + \right.$$
$$\left.\left\{k_f(p-b)^2 + k_r b^2 + k_y x_{f1}^2 + k_y x_{r1}^2\right\} \quad 0 \quad 0 \quad 0 \quad 0 \quad j\omega c_r b + k_r b \quad -j\omega c_f(p-b) - k_f(p-b)\right]^T,$$
$$F_3 = \left[-j\omega c_f - k_f \quad -j\omega c_f(p-b) - k_f(p-b) \quad 0 \quad 0 \quad 0 \quad 0 \quad 0 \quad -m_f\omega^2 + j\omega\left(c_f + c_{pf}\right) + \left(k_f + k_{pf}\right)\right]^T,$$
$$F_4 = \left[0 \quad 0 \quad f_{sa1} \quad f_{sa2} \quad f_{sa1} - f_{sa2} \quad -\omega^2 m_r - f_{sa1} \quad -f_{sa2} \quad 0\right]^T,$$
$$F_5 = \left[-j\omega c_r - k_r \quad j\omega c_r b + k_r b \quad f_{sa2} \quad f_{sa3} \quad f_{sa2} + f_{sa3} \quad -f_{sa2} \quad -\omega^2 m_r + j\omega\left(c_{pr} + c_r\right) + k_{pr} + k_r - f_{sa3} \quad 0\right]^T,$$
$$F_6 = \left[0 \quad 0 \quad -f_{sa1} - \omega^2 m_p + 2k_x \quad -f_{sa2} \quad -f_{sa1} + f_{sa2} - k_x y_{f1} + k_x y_{r1} \quad -f_{sa1} \quad f_{sa2} \quad 0\right]^T,$$
$$F_7 = \left[0 \quad 0 \quad -f_{sa2} \quad -f_{sa3} - \omega^2 m_p + 2k_y \quad -f_{sa2} + f_{sa3} + k_y x_{f1} - k_y x_{r1} \quad f_{sa2} \quad f_{sa3} \quad 0\right]^T,$$
$$F_8 = [0 \quad 0 \quad -f_{sa1} y_{sa} + f_{sa2} x_{sa} \quad -f_{sa2} y_{sa} + f_{sa3} x_{sa} + k_y x_{f1} - k_y x_{r1}$$
$$-f_{sa1} y_{sa} + f_{sa2} x_{sa} + f_{sa2} y_{sa} - f_{sa3} x_{sa} - \omega^2 I_p + k_x y_{f1}^2 + k_y x_{f1}^2 + k_x y_{r1}^2 + k_y x_{r1}^2$$
$$f_{sa1} y_{sa} - f_{sa2} x_{sa} \quad f_{sa2} y_{sa} - f_{sa3} x_{sa} \quad 0]^T.$$

3. RESULTS

The model presented in Section 2 has been used for multiple simulations in this section. Some of the motorcycle parameters have been adapted from existing literature[2] while the engine mount parameters have been adapted from other studies.[4,5] The following parameters were used for all the simulations presented in this section: $p = 1.4$ m, $b = 0.7$ m, $m = 200$ kg, $I = 38$ kg-m^2, $k_f = 15$ kN/m, $k_r = 24$ kN/m, $k_{pf} = 180$ kN/m, $k_{pr} = 180$ kN/m, $m_f = 15$ kg, $m_r = 18$ kg, $m_p = 125$ kg, $I_p = 8$ kg-m^2, $x_{r1} = 320$ mm, $y_{r1} = 55$ mm, $x_{f1} = 325$ mm, $y_{f1} = 20$ mm, $x_{sa} = 270$ mm, $y_{sa} = 30$ mm. The following data was used for the engine mounting system: $E_0 = 5.5$ kPa, $E_{\alpha y} = 0.23$ kPa, $E_{\beta y} = 331$ kPa, $E_{\alpha x} = 0.23$ kPa, $E_{\beta x} = 331$ kPa, $\alpha = 0.66, \beta = 0.07$, $\tau = 1$ s, $\rho = 1100$ kg/m^3, $A = 0.0025$ m^2, $h = 50$ mm.

The first simulation presents transmissibility results of the sprung mass and the two unsprung masses when the motorcycle is traveling over a bump course with varying bump amplitudes at different velocities. The results for the two unsprung masses are shown in Figures 3 and 4 while the results for the sprung mass bounce are shown in Figure 5. A sinusoidal bump course with an amplitude of 30 mm at three distinct speeds (low, intermediate, and high) was used as the excitation input from the road surface. Sprung mass bounce acceleration has also been evaluated and is shown in Figure 6 for the intermediate speed only. As can be observed from Figures 3 and 4, the front and rear unsprung masses exhibit high transmissibility up to 20 Hz regardless of the speed. This can be attributed to the hop modes of the unsprung masses and is comparable to other results of planar dynamics in the literature.[4] Furthermore, transmissibility is seen to be relatively higher at the lower speed of 10 m/s since it corresponds to a relatively lower wavelength of the bump course of the road profile.

The distinctions between the transmissibility of the front and rear unsprung hop in Figures 3 and 4 can be attributed to their natural modes and the nature of their coupling to the sprung mass. While the front unsprung mass is directly connected to the sprung mass, the rear unsprung mass is connected to the powertrain through the swing arm in addition to the direct connection to the sprung mass through the rear suspension. Results for the sprung mass in Figures 5 and 6 exhibit a high transmissibility up to 2 Hz regardless of the speed at which the motorcycle is traveling and a peak of sprung mass bounce acceleration close to 2 Hz. The second peak in the sprung mass transmissibility plot in Figure 5 is seen to have a direct relationship with the vehicle speed, this could be attributed to the coupled bounce and pitch modes of the sprung mass. The nature of the sprung mass transmissibility peak can be directly influenced by the design of the mounting system and sprung mass bounce acceleration can be used as a direct indicator of ride comfort.

The results in Figure 7 demonstrate the essence of the discretized model presented in this paper. The magnitude of the norm of force transmitted to the sprung mass through the engine mounting system can be seen in Figure 7 as the motorcycle travels over a sinusoidal bump course at a velocity of 30 m/s. While a conventional spring-damper representation of the mounting system would successfully capture the initial peak in transmitted force at relatively lower frequencies, the peaks at higher frequencies have been captured in this study by successfully modeling the inertia effect of the mounting system through the discretized model. This may be specifically important for the mounting systems of electric powertrains since they operate at higher speeds and exhibit a high motor order.[5,8] A typical spring-damper model would not be able to model the internal resonances of the mounting system.

The model developed in Section 2 has also been used to analyze the response to excitations from the irregularities of the road surface. The power spectral density (PSD) of a good road surface as well as an average road surface has been used as the input while the motorcycle is traveling in a straight line at a constant velocity. The PSD of a specific road surface can be directly used from the definitions identified in the existing literature.[24] The resulting PSD of the rear unsprung mass hop and the sprung mass bounce and pitch are shown in Figures 8, 9, and 10. As can be observed from Figures 8 to 10, the peak and the bandwidth resulting from the average road surface are higher than the good road surface in all three cases. However, the extent of this increase varies from one mass to another. Although the PSD plots are presented for a velocity of 10 m/s only, other speeds yielded similar trends.

The rear unsprung hop PSD is seen to peak at 20 Hz with a relatively higher bandwidth for the average road surface. The

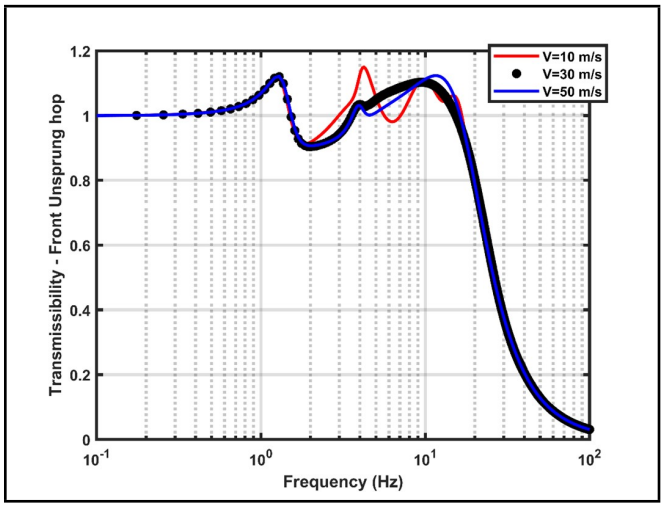

Figure 3. Displacement Transmissibility — Front unsprung mass hop.

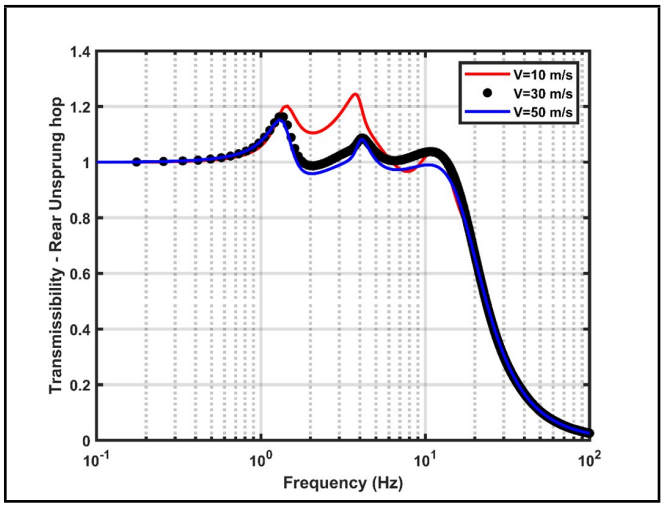

Figure 4. Displacement Transmissibility — Rear unsprung mass hop.

rear unsprung hop is coupled to the dynamics of the mounting system due to the swing arm connecting the rear unsprung mass to the powertrain, as can be seen from the layout of the model in Figure 1. Therefore, this coupling could have implications for the planar handling of the motorcycle that can be evaluated from the PSD of the rear unsprung hop. This contrasts with the front unsprung hop since the front unsprung mass is directly connected to the sprung mass through the front suspension system.

As can be seen from the sprung mass PSD results in Figures 9 and 10, the peaks for pitch and bounce are within a narrow range of frequencies with relatively limited bandwidth. This is directly related to the mounting system and the discretized representation of the mounting system used in this study. It can be observed from a comparison of the sprung mass results with a similar motorcycle with an internal combustion engine that the peaks of power spectral density are shifted. This will need to be investigated and experimentally evaluated to comprehend ride comfort and planar handling in motorcycles with electric powertrains.

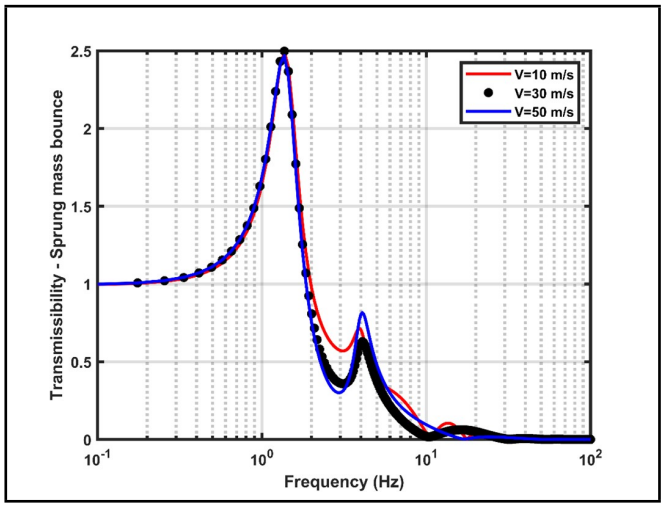

Figure 5. Displacement Transmissibility — Sprung mass bounce.

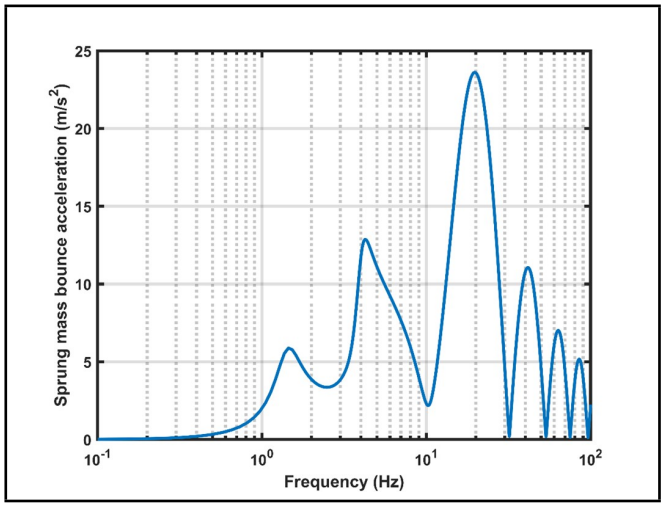

Figure 6. Sprung mass bounce acceleration ($V = 30$ m/s).

4. CONCLUSIONS

In this paper, a planar model of a motorcycle has been developed and investigated to examine the influence of the inertia effect of the mounting system of an electric powertrain. The model derived for this study consists of eight degrees-of-freedom along with a discretized representation of the mounting system. This model can analyze displacement transmissibility as well as ride comfort and planar handling while the motorcycle is traveling in a straight line. The proposed model is specifically useful for investigating the influence of parameters associated with the mounting system and the suspension system on ride comfort. Since an electric powertrain is typically associated with relatively higher frequencies, representation of the mass and elasticity of the mounting system is important to model the inertia effect. The model presented in this paper is successful in capturing high frequency characteristics, that are well above 1 kHz, and internal resonances of the mounting system.

Transmissibility results indicate the inherent coupling between sprung mass pitch and bounce and the influence of vehicle speed while the motorcycle is driving in a straight line on a bump course. The power spectral density (PSD) results

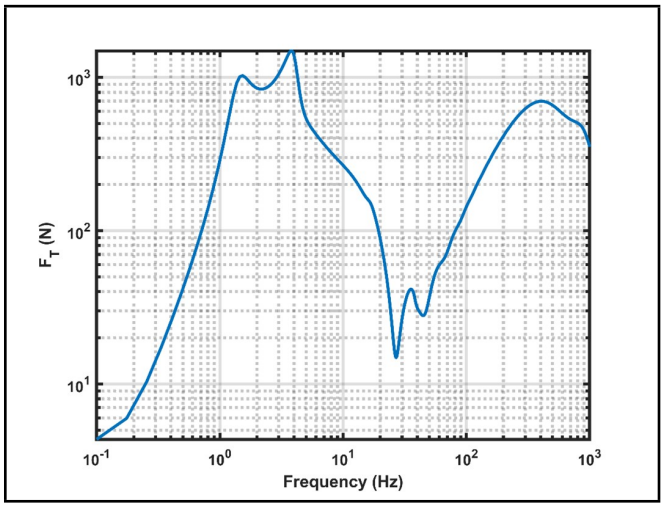

Figure 7. Transmitted force — sprung mass ($V = 30$ m/s).

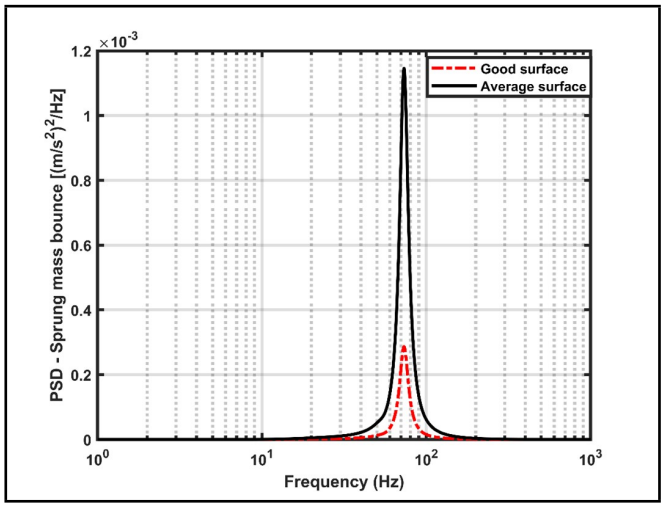

Figure 9. Power spectral density — Sprung mass bounce ($V = 10$ m/s).

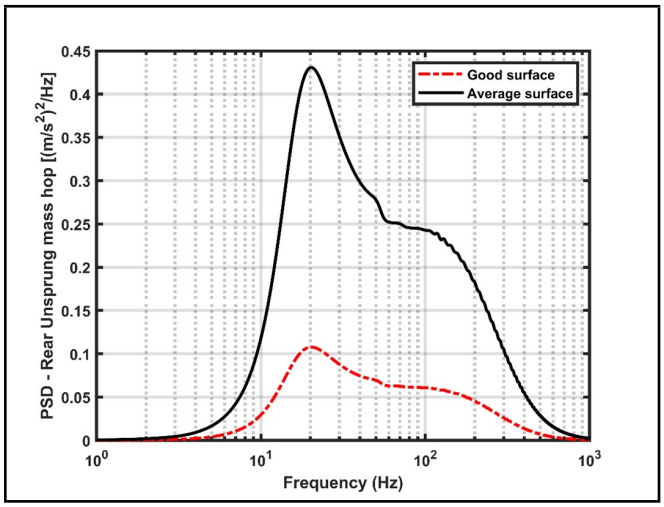

Figure 8. Power spectral density — Rear unsprung mass hop ($V = 10$ m/s).

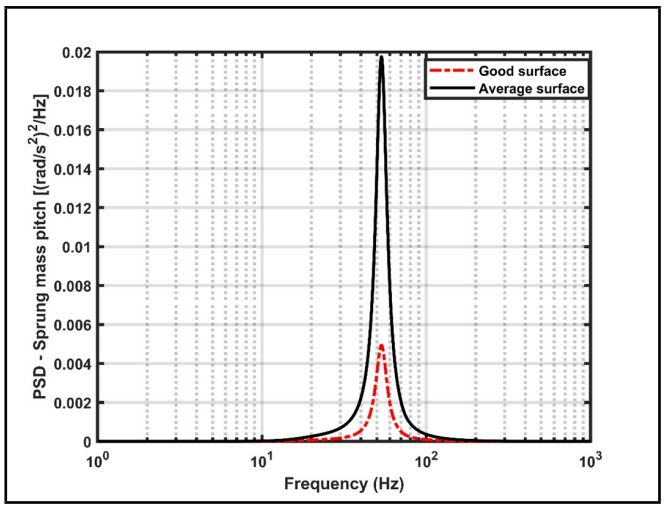

Figure 10. Power spectral density — Sprung mass pitch ($V = 10$ m/s).

indicate a shift of the peaks for the sprung mass in a motorcycle with an electric powertrain. On the other hand, the unsprung mass PSD results are like other comparable vehicles in the literature.[4] It can be observed from the results that force transmitted to the sprung mass through the mounting system clearly captures the resonance of the mounting system at relatively higher frequencies. This indicates that the model is successful in capturing the inertia effect of the mounting system.

Future studies will investigate the impact of different mounting system layouts on the planar dynamics of a motorcycle with an electric powertrain. Since there are a few different kinds of electric motors that are commonly used by manufacturers, distinctions between these motors and their implications on the mounting systems will be analyzed in future work. Experimental evaluation will also be performed for model correlation and validation. Experimental data is expected to be particularly beneficial for validating the discretized model of the mounting system and for determining an optimal mounting system layout with constraints that are specific to electric powertrains.

REFERENCES

[1] V. Cossalter, A. Doria, S. Garbin, and R. Lot, Frequency-domain method for evaluating the ride comfort of a motorcycle, *Vehicle System Dynamics*, **44**, 339–355, (2006). https://doi.org/10.1080/00423110500420712

[2] V. Cossalter, Motorcycle Dynamics, Second Edition, Lulu, Morrisville, NC, USA, (2006).

[3] S. Kaul and A. K. Dhingra, Engine mount optimization for vibration isolation in motorcycles, *Vehicle System Dynamics*, **47**, 419–436, (2009). https://doi.org/10.1080/00423110802167458

[4] S. Kaul, Influence of a Vibration Isolation System on Planar Dynamics of a Motorcycle, *International Journal of Acoustics and Vibration*, **25**, 96–103, (2020). https://doi.org/10.20855/ijav.2020.25.11603

[5] A. Lion and M. Johlitz, A mechanical model to describe the vibroacoustic behaviour of elastomeric engine mounts for electric vehicles, *Mechanical Sys-*

tems and Signal Processing, **144**, 106874, (2020). https://doi.org/10.1016/j.ymssp.2020.106874

[6] S. Kaul, Multi-degree-of-freedom Modeling for Electric Powertrains: Inertia Effect of Engine Mounting System, *Proceedings of the ASME International Mechanical Engineering Congress and Exposition*, IMECE2021-66287, (2021). https://doi.org/10.1115/imece2021-66287

[7] P. Enge, N. Enge, and S. Zoepf, Electric Vehicle Engineering, McGraw Hill, New York, NY, USA, (2021).

[8] W. Deng and S. Zuo, Electromagnetic Vibration and Noise of Permanent-Magnet Synchronous Motors for Electric Vehicles: An Overview, *IEEE Transactions on Transportation Electrification*, **5**, 59–70, (2019). https://doi.org/10.1109/tte.2018.2875481

[9] K. Qian, J. Wang, Y. Gao, Q. Sun, and J. Liang, Interior noise and vibration prediction of permanent magnet synchronous motor, *Journal of Vibroengineering*, **20**, 2225–2236, (2018). https://doi.org/10.21595/jve.2018.18605

[10] Y. Qin, X. Tang, T. Jia, Z. Duan, J. Zhang, Y. Li, and L. Zheng, Noise and vibration suppression in hybrid electric vehicles, *Renewable and Sustainable Energy Reviews*, **124**, 109782, (2020). https://doi.org/10.1016/j.rser.2020.109782

[11] Z. Cao, A. Mahmoudi, S. Kahourzade, and W. L. Soong, An Overview of Electric Motors for Electric Vehicles, *IEEE 31st Australasian Universities Power Engineering Conference (AUPEC)*, AUPEC52110-2021, (2021). https://doi.org/10.1109/aupec52110.2021.9597739

[12] C. Thunberg and H. Wapling, Technical Concept Study of an Electric Motorcycle Powertrain: Product Development and Initial Design, Master's Thesis, Chalmers University of Technology, Gothenburg, Sweden, (2023).

[13] Mechanical Simulation Corp, BikeSim, Ann Arbor, MI, USA, (2017).

[14] Dynamotion Srl, FastBike, Padova, Italy, (2017).

[15] G. Rane and S. Deshmukh, Development of Mount for Electric Powertrains — A Multi Degree of Freedom Optimization Approach, *SAE Technical Paper*, 2020-01-0417, (2020). https://doi.org/10.4271/2020-01-0417

[16] S. Kaul, Engine Mounting Systems for Electric Powertrains: Mounting Layouts and Design Parameters, *Proceedings of the ASME International Mechanical Engineering Congress and Exposition*, IMECE2022-87646, (2022). https://doi.org/10.1115/imece2022-87646

[17] X. Zeng, J. Liette, S. Noll, and R. Singh, Analysis of Motor Vibration Isolation System with Focus on Mount Resonances for Application to Electric Vehicles, *SAE Journal of Alternative Powertrains*, **4**, 370–377, (2015). https://doi.org/10.4271/2015-01-2364

[18] A. J. Tuononen and A. Lajunen, Modal analysis of different drivetrain configurations in electric vehicles, *Journal of Vibration and Control*, **24**, 126–136, (2018). https://doi.org/10.1177/1077546316635857

[19] Q. Wang, K. Rajashekara, Y. Jia, and J. Sun, A Real-Time Vibration Suppression Strategy in Electric Vehicles, *IEEE Transactions on Vehicular Technology*, **66**, 7722–7729, (2017). https://doi.org/10.1109/tvt.2017.2688416

[20] F. Xin, L. Qian, H. Du, and W. Li, Multi-objective robust optimization design for powertrain mount system of electric vehicles, *Journal of Low Frequency Noise, Vibration and Active Control*, **36**, 243–260, (2017). https://doi.org/10.1177/0263092317719635

[21] J. Bucha, J. Danko, T. Milesich, T. Nemec, and L. Magdolen, Comparison of FEM Simulations of Rubber-Metal Mount Element, *Journal of Mechanical Engineering*, **72**, 15–22, (2022). https://doi.org/10.2478/scjme-2022-0002

[22] A. Masa'id, B. W. Lenggana, U. Ubaidillah, D. D. Susilo, and S. -B. Choi, A review on vibration control strategies using magnetorheological materials actuators: Application perspective, *Actuators*, **12**, 113, (2023). https://doi.org/10.3390/act12030113

[23] D. Nurkertamanda, W. Budiawan, Z. A. Zahra, and R. J. Gitowardojo, Experimental design for a sustainable society among motorcyclists: The influence of road types and speeds on whole-body vibration exposure and musculoskeletal disorders in motorcyclists, *Multidisciplinary Science Journal*, **7**, 2025053, (2025). https://doi.org/10.31893/multiscience.2025053

[24] Y. Matsuda, T. Murase, and D. Kawai, The Feasibility Study of a Design Concept of Electric Motorcycle, *SAE Technical Paper*, 2015-01-1775, (2015). https://doi.org/10.4271/2015-01-1775

[25] N. Dal Bianco, R. Lot, and K. Matthys, Lap time simulation and design optimisation of a brushed DC electric motorcycle for the Isle of Man TT Zero Challenge, *Vehicle System Dynamics*, **56**, 27–54, (2018). https://doi.org/10.1080/00423114.2017.1342847

[26] S. Kaul, Modeling and Analysis of Passive Vibration Isolation Systems, Elsevier, Cambridge, MA, USA, (2021).

[27] L. Sun, On Human Perception and Evaluation to Road Surfaces, *Journal of Sound and Vibration*, **247**, 547–560, (2001). https://doi.org/10.1006/jsvi.2001.3642